A Dynamic Frequency Sweeping Based Parameter Estimation Method for Wireless Power Transfer

Zhu, Gangwei; Dong, Jianning; Bauer, Pavol

DOI
10.1109/IECON51785.2023.10311772

Publication date
2023

Document Version
Final published version

Published in
Proceedings of the IECON 2023- 49th Annual Conference of the IEEE Industrial Electronics Society

Citation (APA)
Zhu, G., Dong, J., & Bauer, P. (2023). A Dynamic Frequency Sweeping Based Parameter Estimation Method for Wireless Power Transfer. In *Proceedings of the IECON 2023- 49th Annual Conference of the IEEE Industrial Electronics Society* (Proceedings of the Annual Conference of the IEEE Industrial Electronics Society). IEEE. https://doi.org/10.1109/IECON51785.2023.10311772

A Dynamic Frequency Sweeping Based Parameter Estimation Method for Wireless Power Transfer

1st Gangwei Zhu
Department of Electrical Engineering,
Mathematics and Computer Science
Delft University of Technology
Delft, the Netherlands
G.Zhu-2@tudelft.nl

2nd Jianning Dong
Department of Electrical Engineering,
Mathematics and Computer Science
Delft University of Technology
Delft, the Netherlands
J.Dong-4@tudelft.nl

3rd Pavol Bauer
Department of Electrical Engineering,
Mathematics and Computer Science
Delft University of Technology
Delft, the Netherlands
P.Bauer@tudelft.nl

IECON 2023- 49th Annual Conference of the IEEE Industrial Electronics Society | 979-8-3503-3182-0/23/$31.00 ©2023 IEEE | DOI: 10.1109/IECON51785.2023.10311772

Abstract*—It is ideal for the wireless power transfer (WPT) systems to operate at the resonance state for better transmission performance. In practice, however, the parameters of the resonant circuits often deviate because of the capacitance drift and coil misalignment. To this end, this paper proposes a new parameter estimation method for the WPT systems, which is able to facilitate the power flow control and active impedance tuning of the WPT systems under parameter deviations. Distinct from the traditional parameter identification methods , the proposed method is implemented with an short-circuited rectifier, and therefore, the whole estimation process is independent of the load variations. Furthermore, to avoid severe system detuning during the frequency-sweeping process, a dynamic frequency sweeping method is proposed to efficiently and safely extract the data of the primary and secondary coil currents. Based on the extracted data, a mathematical model is established, and the JAYA algorithm is utilized to identify the unknown parameters. Experimental results are presented to verify the estimation accuracy of the proposed method.

***Index Terms*—wireless power transfer, parameter estimation, the JAYA algorithm**

I. INTRODUCTION

Wireless power transfer (WPT) is regarded as a promising charging solution for many industrial applications, such as consumer electronics, underwater devices, medical equipment and electrified transportation [1]–[4]. For the WPT systems, the coils can be regarded as a loosely coupled transformer, and the compensation for the leakage inductances is important. Among all of the existing compensation topologies, the SS compensation is the most commonly-used topology due to its simple structure and the load-independent output current characteristic [5]. For the SS compensation, the compensation capacitors are designed to be resonant with the self-inductances of the coupled coils at the designed resonant frequency. For instance, 85 kHz is usually selected as the resonant frequency in many applications. However, in practice, it is challenging to ensure that the system works in the resonance state due to the parameter deviations caused by capacitance drift and coil displacement. Since the deviations of these parameters are inevitable and unpredictable, the WPT systems may work in a non-resonance state, resulting in reduced efficiency and lower power factor [6]. From another point of view, if these unknown parameters can be estimated, then the active impedance tuning can be implemented to enable the system works at resonance. Additionally, the estimation of the mutual inductance also plays an important role in achieving optimal power flow control and maximum efficiency tracking for the WPT systems.

In recent years, many research efforts have been devoted to the parameter estimation of the WPT systems, most of which are based on the frequency sweeping. In [7], Yin *et al.* presented a primary-side monitoring method to estimate multiple loads for the multi-coil WPT systems. Furthermore, in [8], Yin *et al.* extended their work to identify the mutual inductance and load resistance. By scanning the operating frequency around the resonant frequency, the mutual inductance and the load conditions are estimated with only the primary-side voltage and current. It should be noted that in [7] and [8], the least square approximation (LSA) algorithm is used to find the optimal solutions. However, according to the analysis in [9], the method based on the heuristic algorithm is able to obtain the optimal solutions more efficiently than the LSA for the systems with multiple variables. As a result, the genetic algorithm (GA) is firstly introduced in [10] to estimate the unknown parameters. Nevertheless, for the GA algorithm, several algorithm-specific parameters, i.e., the crossover and mutation rates, is required to be adjusted manually. For this reason, the adaptive differential evolution (ADE) algorithm is then proposed in [9]. Based on the fitness values of the individuals, the crossover and mutation rates are adaptively tuned in each iteration. However, the crossover and mutation rates are required to be updated in each iteration, resulting in an increased computational complexity. In [11], a gradient descent method is adopted to obtain the optimal solutions. However, this method needs to solve the partial differential for each unknown parameter, which significantly increases the difficulty of mathematical modelling.

On the other hand, the traditional frequency-sweep-based methods generally sweep the frequency near the resonant frequency point [7]–[11], which may lead to severe system detuning when the parameters of the resonant circuits and the load conditions vary in a wide range. Such severe system detuning results in remarkable coil currents and power fluctuations, jeopardizing the safe operation of the system.

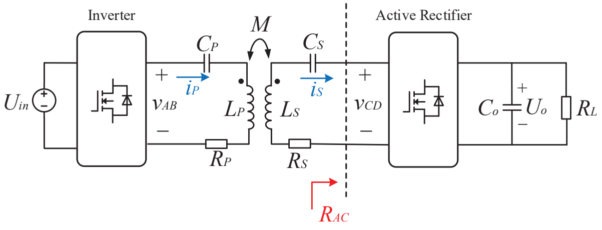

Fig. 1. Topology of the investigated WPT system.

To address the above issues, a new parameter estimation method is proposed to identify all the unknown parameters of the resonant circuits. With the rectifier short-circuited during the parameter estimation process, the proposed method prevents significant power fluctuations caused by the frequency sweeping. Subsequently, a dynamic frequency sweeping method is proposed to extract the required data under multiple frequency points. Finally, a simple and easy-to-follow heuristic method, i.e., the JAYA algorithm, is incorporated to estimate the unknown parameters. Experimental results are presented to validate the effectiveness of this work.

II. PROBLEM FORMULATION

The most-commonly used series-series (SS) compensation topology is utilized in the studied WPT system, as illustrated in Fig. 1. Moreover, an active rectifier is employed in the receiver side. The active rectifier enables the dual-side control [12], bidirectional power flow [13], maximum efficiency tracking [14], and active impedance tuning [15], which has attracted more and more attention from the researchers in the field of WPT. In this paper, the active rectifier is also considered to implement the proposed method. Moreover, in Fig. 1, the compensation capacitors C_P and C_S are adopted to compensate the coil self-inductances L_P and L_S. R_P and R_S are the loss resistance of the primary and secondary resonant circuits, while R_L is the load resistance. R_{AC} represents the equivalent resistance seen from the ac-side of the rectifier. The dc input and output voltages are denoted by U_{in} and U_o, while i_P and i_S indicate the coil currents on the primary and secondary sides, respectively. The mutual inductance is given by $M = k\sqrt{L_P L_S}$, where k is the coupling factor of the coils.

In the real applications, due to the coil misalignment and capacitance drift, the parameters of L_P, L_S, C_P, and C_S may vary significantly, resulting in an impedance mismatch of the resonant circuits. On the other hand, the information of M is also very important in the power flow control. Therefore, it is preferred to estimate all of the unknown parameters to facilitate active impedance tuning and optimal power flow control for the WPT systems.

In order to estimate multiple unknown variables, traditional parameter estimation methods acquire the required data by scanning the frequency near the resonant frequency. Nevertheless, when the deviations of the system parameters vary in a wide range, severe system detuning may occur due to the frequency variations. Considering both the impact of capacitance drift and coil misalignment in the real applications, the detailed parameters of the studied system are illustrated in Table I. In Table I, f_N is the nominal resonant frequency, while D is the air gap between the primary and secondary coils. To investigate the influence of coil misalignment, the air gap D is varied between 10 and 15 cm. Due to the variation of the air gap, the parameters of L_P, L_S, and k are also varied, as shown in Table I. Moreover, in Table I, the nominal values of the compensation capacitors are denoted by C_{P0} and C_{S0}, while d_P and d_S represent their corresponding degrees of capacitance drift. The actual primary and secondary capacitances, therefore, can be given by $C_P = (1 + d_P)C_{P0}$ and $C_S = (1 + d_S)C_{S0}$, respectively.

TABLE I
PARAMETERS OF THE INVESTIGATED WPT SYSTEM

Symbol	Value	Symbol	Value
L_P	327.5 $\sim$ 335.5 μH	L_S	216.5 $\sim$ 222.7 μH
k	0.22 $\sim$ 0.35	D	10 $\sim$ 15 cm
C_{P0}	10.45 nF	C_{S0}	15.74 nF
d_P	-0.2 $\sim$ 0.2	d_S	-0.2 $\sim$ 0.2
R_L	100 Ω	R_{AC}	5 $\sim$ 81 Ω
U_{in}	200 V	f_N	85 kHz

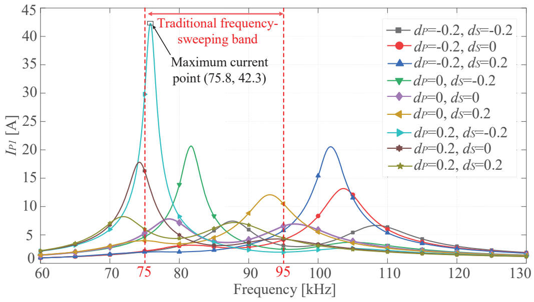

Fig. 2. Value of I_{P1} under the combined effects of capacitance drift and frequency variations in the case of $R_{AC} = 20\ \Omega, k = 0.22$.

Based on the parameters listed in Table I, the RMS value of the fundamental primary coil current, namely I_{P1}, is investigated at varying frequencies. Fig. 2 presents an example of how I_{P1} varies under the combined effects of capacitance drift and frequency variations. In Fig. 2, the conventional frequency-sweeping band is set as 75 $\sim$ 95 kHz to guarantee that sufficient frequency points can be swept. When there is no drift in the capacitors, as shown in the purple line of Fig. 2, the variation of the coil currents caused by the frequency variations are relatively small. However, when the values of the capacitor vary in a wide range, the frequency variations lead to significantly increased coil currents. Specifically, under the case of d_P=0.2, d_S=-0.2, the maximum value of I_{P1} reaches 42.3 A at 75.8 kHz.

It should be mentioned that Fig. 2 only presents the results under the case of $R_{AC} = 20\ \Omega, k = 0.22$ as an example. To further demonstrate the influence of the coupling changes and load variations, the maximum value of I_{P1} under different values of R_{AC} and k is visualized in Fig. 3. As shown in Fig. 3, the maximum value of I_{P1} is inversely related to R_{AC} and

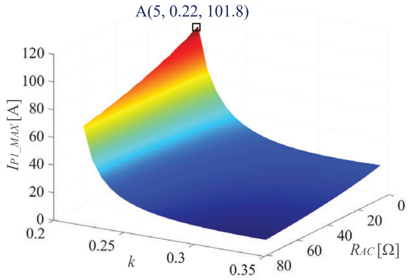

Fig. 3. Maximum value of I_{P1} under different values of R_{AC} and k.

k. This indicates that when R_{AC} and k are small, more severe system detuning may occur due to the frequency scanning. The worst case in Fig. 3 is under the case of $R_{AC} = 5\ \Omega$ and $k = 0.22$, where the maximum value of I_{P1} reaches more than 100 A.

Based on the above analysis, when the parameters of the resonant circuits and the load conditions deviate in a large range, sweeping the frequency around the resonant point may dramatically increase the value of the coil currents, jeopardizing the safe operation of the system. Therefore, if the parameters of the resonant circuits and the load conditions vary in a large range, it is not preferred to directly use the traditional frequency-sweeping-based parameter estimation methods.

III. PROPOSED PARAMETER ESTIMATION METHOD

To address the abovementioned issue, we propose a novel parameter estimation method to identify all of the unknown parameters of the resonant circuits, including L_P, L_S, C_P, C_S and M. The block diagram of the proposed method is illustrated in Fig. 4. The proposed method is implemented with an short-circuited rectifier to prevent significant load power fluctuations arisen from the frequency scanning. The short-circuited rectifier is achieved by constantly turning on the power switches Q_1, Q_3, and consistently turning off the power switches Q_2, Q_4. Furthermore, the coil currents i_P and i_S are measured through two separate current sensors. The low pass filters (LPFs) are employed to extract the fundamental components of i_P and i_S. Subsequently, the RMS values of i_{P1} and i_{S1} are calculated. The measured secondary information is transmitted to the primary side via a wireless communication module. Based on the values of I_{P1} and I_{S1}, a dynamic frequency sweeping method is carried out to dynamically tune the operating frequency. By measuring I_{P1} and I_{S1} at multiple frequency points, the required data for parameter estimation is obtained. Finally, based on the obtained data, the unknown parameters are calculated by the JAYA algorithm. The implementation details of the proposed method will be elaborated in this section.

A. Mathematical Model

With a short-circuited rectifier, as shown in Fig. 4, the equivalent circuit model of the WPT system is illustrated in Fig. 5. In Fig. 5, ω is the operating angular frequency; $\dot{V}_{P1}$ is the phasor form of the fundamental component of v_{AB}; $\dot{I}_{P1}$ and $\dot{I}_{S1}$ are the phasor form of the fundamental components of i_P and i_S, respectively. Based on Fig. 5, the equivalent input impedance of the resonant circuits can be deduced by

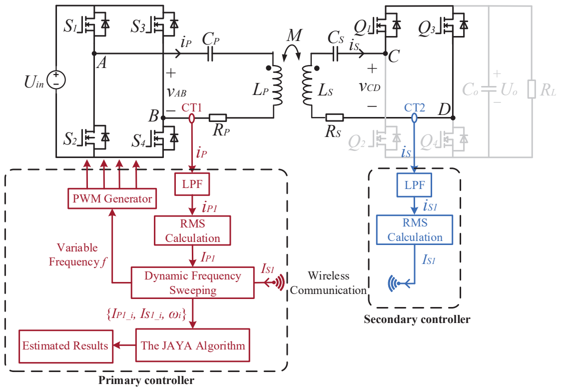

Fig. 4. Block diagram of the proposed parameter estimation method.

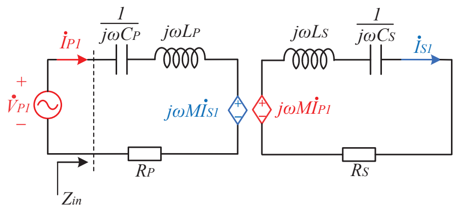

Fig. 5. Equivalent model of the WPT system with a short-circuited rectifier.

$$Z_{in} = R_P + j(\omega L_P - \frac{1}{\omega C_P}) + \frac{(\omega M)^2}{R_S + j[\omega L_S - 1/(\omega C_S)]}, \tag{1}$$

Observing (1) reveals that Z_{in} varies with the operating frequency ω. This means that if the operating frequency ω is adjusted to another value, a new value of Z_{in} can be acquired. According to the analysis in [7] and [8], by adjusting the frequency ω at different points, multiple sets of $\{\omega_i, |Z_{in\_i}|\}$ can be derived as

$$|Z_{in\_i}| = \frac{V_{P1\_i}}{I_{P1\_i}} = f(R_P, R_S, L_P, L_S, C_P, C_S, M, \omega_i), \tag{2}$$

where $\omega_i (i = 1, 2, \cdots, m)$ represent the i-th frequency point; m is the number of the measured frequency points; V_{P1_i} and I_{P1_i} are the RMS values of $\dot{V}_{P1}$ and $\dot{I}_{P1}$ at the i-th frequency point.

The input impedance model described in (2) is widely-used in the front-end parameter monitoring [7]–[11]. However, according to the analysis in [11], if only adopting the primary-side information, the parameters of $\{L_S, C_S, M\}$ cannot be accurately estimated. Therefore, in this paper, the secondary-side information is also introduced, and the equivalent gain from I_{S1} to V_{P1} is derived by

$$Z_{PS} = \frac{V_{P1}}{I_{S1}} = j\omega M - \frac{(R_P + jX_P)(R_S + jX_S)}{j\omega M}. \tag{3}$$

By adjusting the frequency ω, multiple sets of $\{\omega_i, |Z_{PS\_i}|\}$

can also be obtained as

$$|Z_{PS\_i}| = \frac{V_{P1\_i}}{I_{S1\_i}} = g(R_P, R_S, L_P, L_S, C_P, C_S, M, \omega_i). \tag{4}$$

Furthermore, based on (2) and (4), the mathematical model for the parameter estimation is established as

$$\min J = ||\boldsymbol{V_{P1}} - \boldsymbol{V_{P1est}}|| + ||\boldsymbol{V_{P1}} - \boldsymbol{\hat{V}_{P1est}}|| \tag{5}$$

s.t. $\boldsymbol{V_{P1est}} = |\boldsymbol{Z_{in}}|\boldsymbol{I_{P1}}$, $\boldsymbol{\hat{V}_{P1est}} = |\boldsymbol{Z_{PS}}|\boldsymbol{I_{S1}}$, $L_{PL} \leq L_P \leq L_{PH}$, $L_{SL} \leq L_S \leq L_{SH}$, $C_{PL} \leq C_P \leq C_{PH}$, $C_{SL} \leq C_S \leq C_{SH}$, and $M_L \leq M \leq M_H$, where

$$\left\{\begin{array}{rcl} |\boldsymbol{Z_{in}}| & = & diag\{|Z_{in\_i}|\}(i = 1, \cdots, m), \\ |\boldsymbol{Z_{PS}}| & = & diag\{|Z_{PS\_i}|\}(i = 1, \cdots, m), \\ \boldsymbol{I_{P1}} & = & [I_{P1\_1}, I_{P1\_2}, \cdots, I_{P1\_m}], \\ \boldsymbol{I_{S1}} & = & [I_{S1\_1}, I_{S1\_2}, \cdots, I_{S1\_m}], \\ \boldsymbol{V_{P1est}} & = & [V_{P1est\_1}, V_{P1est\_2}, \cdots, V_{P1est\_m}], \\ \boldsymbol{\hat{V}_{P1est}} & = & [\hat{V}_{P1est\_1}, \hat{V}_{P1est\_2}, \cdots, \hat{V}_{P1est\_m}], \\ \boldsymbol{V_{P1}} & = & [V_{P1\_1}, V_{P1\_2}, \cdots, V_{P1\_m}]. \end{array}\right.$$

Herein, $\boldsymbol{I_{P1}}$ and $\boldsymbol{I_{S1}}$ are the measured RMS values of i_{P1} and i_{S1}; $\boldsymbol{V_{P1est}}$ and $\boldsymbol{\hat{V}_{P1est}}$ are the estimated RMS values of v_{P1} derived by $|\boldsymbol{Z_{in}}|\boldsymbol{I_{P1}}$ and $|\boldsymbol{Z_{PS}}|\boldsymbol{I_{S1}}$, respectively; $\boldsymbol{V_{P1}}$ is the measured RMS values of v_{P1}.

B. Proposed Dynamic Frequency Sweeping Method

As demonstrated in the section III-A, the operating frequency ω needs to be adjusted to multiple points to obtain different values of Z_{in} and Z_{PS}. In traditional frequency-sweeping-based parameter estimation method, the operating frequency is swept around the resonant point in a fixed interval. For instance, in [9], the operating frequency is swept from 90 to 110 kHz at an interval of 1 kHz, and the resonant frequency is 100 kHz. Nevertheless, based on the analysis in section II, when the parameters of the resonant circuits and the load conditions vary in a wide range, varying the frequency near the resonant point may cause severe system detuning and significantly increased coil currents. Therefore, we propose a dynamic frequency sweeping method to obtain the required frequency points, as illustrated in Fig. 6. Distinct from the traditional methods, we adjust the frequency from a lower bound f_L and a upper bound f_H. The frequency is firstly increased from the lower bound f_L and the process is stopped when I_{P1} or I_{S1} exceeds the threshold value I_M. It is worthy noting that the threshold value I_M is determined by the current capability of the system. Subsequently, the frequency is decreased from the upper bound f_H and the process is terminated when I_{P1} or I_{S1} is again greater than I_M. In this paper, according to the system parameters, I_M is set to 10 A, while f_L and f_H are configured at 65 kHz and 125 kHz, respectively.

Additionally, it should be noted that the frequency interval is not fixed but dynamically tuned according to the measured values of the coil currents. There are two reasons why we consider a dynamic interval. Firstly, when the frequency approaches to the threshold current, as shown in Fig. 7, the curves of the coil currents become extremely steep. If a large frequency interval is implemented under this case, the coil currents may greatly exceed the threshold. Take $d_P = d_S = 0.2$ under the case of D=15 cm as an example, as shown in Fig. 7, I_{P1} is 9.2 A when the frequency is 69 kHz, whereas it rapidly increases to 15.7 A at 70 kHz. On the other hand, when the frequency is in the neighbourhood of f_L and f_H, as shown in Fig. 7, the coil currents are relatively low, and the corresponding current curves are more flat. This implies that when the coil currents are low, small frequency intervals will result in a long duration for the sweeping process. Therefore, considering the above two reasons, a dynamic frequency interval is implemented. The update formulas for the proposed dynamic frequency sweeping method are as follows.

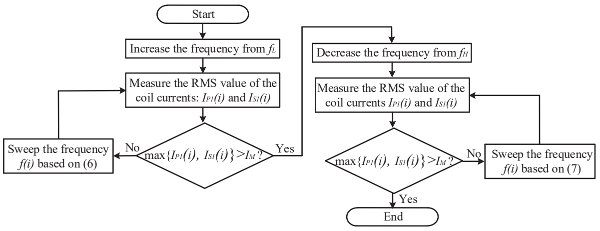

Fig. 6. Flow chart of the proposed dynamic frequency sweeping method.

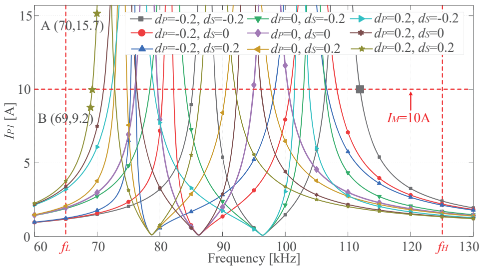

Fig. 7. Value of I_{P1} when the rectifier output is short-circuited under the case of $D = 15\ cm$.

$$f(i+1) = f(i) + \tau \times ceil[I_M - \max(I_{P1}(i), I_{S1}(i))], \tag{6}$$

$$f(i+1) = f(i) - \tau \times ceil[I_M - \max(I_{P1}(i), I_{S1}(i))]. \tag{7}$$

Herein, (6) indicates the frequency update formula when the frequency is increased from f_L, while (7) represents the update formula when the frequency is decreased from f_H. Moreover, $ceil$ is the round-up function; τ is a fixed factor, which is configured at 0.2. As it can be observed from (6) and (7), the frequency interval is dynamically tuned between 0.2 kHz and 2 kHz based on the measured I_{P1} and I_{S1}. It should be emphasized that in the frequency sweeping process, the maximum value of I_{P1} and I_{S1} is used as the basis for judgment. This means that when the current on one side exceeds the threshold, the sweeping process stops, ensuring safe operation of the both the primary and secondary circuits.

C. Numerical Calculation

Through the proposed dynamic frequency sweeping method, the measured data under multiple frequency points can be acquired. The next step is to utilize the measured data to identify the unknown parameters. This can be achieved by

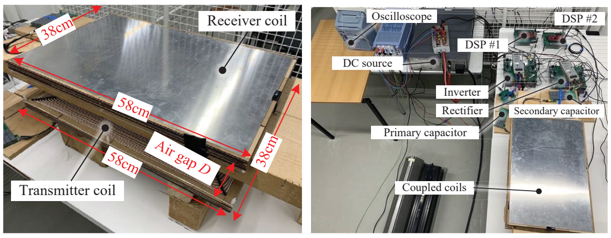

(a) (b)

Fig. 8. Experimental setup: (a) dimensions of the adopted coupled coils, (b) experimental platform for the parameter estimation.

solving (5). Specifically, the optimal solutions that minimize the fitness value in (5) will be regarded as the estimation results. There are many algorithms available for solving the optimization problem described in (5), and the algorithms that are simple and easy to follow are preferred. To this end, the JAYA algorithm, which is proposed by Rao in 2016 [16], is selected in this paper. Compared with the traditional GA and DE algorithms, this method does not require manual tuning of algorithm-specific parameters. Only two general parameters, i.e., the population size P_{size} and the maximum iteration number Gen_{max} are needed to be pre-defined.

The implementation details of the JAYA method are elaborated as follows: **[Initialization]** A random population $\boldsymbol{x}$ with P_{size} individuals is generated in the first iteration, where $\boldsymbol{x_{p,q}}$ is the q-th parameter of the p-th individual ($p = 1, 2, \cdots, P_{size}$; $q = 1, 2, \cdots, N$), and N is the number of the unknown parameters. **[Fitness]** Subsequently, the fitness value of each individual is calculated using (5). **[Update]** Based on the fitness of each individual, the best individual $\boldsymbol{x_{best}} = [x_{best,1}, x_{best,2}, \cdots, x_{best,N}]$ and the worst individual $\boldsymbol{x_{worst}} = [x_{worst,1}, x_{worst,2}, \cdots, x_{worst,N}]$ are utilized to update the population, which is given by

$$\boldsymbol{x'_{p,q}} = \boldsymbol{x_{p,q}} + r_1(\boldsymbol{x_{best,q}} - |\boldsymbol{x_{p,q}}|) - r_2(\boldsymbol{x_{worst,q}} - |\boldsymbol{x_{p,q}}|), \tag{8}$$

where $\boldsymbol{x_{best,q}}$ and $\boldsymbol{x_{worst,q}}$ are the q-th parameter of the best and worst individuals, respectively; r_1 and r_2 are two random numbers within [0,1]. In (8), the term $r_1(\boldsymbol{x_{best,q}} - |\boldsymbol{x_{p,q}}|)$ presents the tendency of the new individual to approach the best individual, whereas the term $-r_2(\boldsymbol{x_{worst,q}} - |\boldsymbol{x_{p,q}}|)$ shows the tendency of escaping from the worst individual. **[Selection]** The updated individual $\boldsymbol{x'_{p,q}}$ is accepted if it gives a better fitness value. All the accepted individuals are adopted as the input of the next iteration. **[Termination]** The optimization process stops when the termination condition is satisfied. Herein, the termination condition is the iteration number reaches Gen_{max}.

IV. EXPERIMENTAL RESULTS

In this section, experimental results are presented to verify the feasibility of the proposed parameter estimation method. The experimental setup is shown in Fig. 8. The detailed parameters of the SS-compensated WPT prototype are already illustrated in Table I. Moreover, a power supply (Delta SM500-CP-90) is adopted to provide the dc input, and the voltage is configured at 200 V. Two H-bridge converters are employed as the primary-side inverter and the secondary-side rectifier, respectively. The PWM signals for the inverter and rectifier are generated by the TI LaunchPads F28379D. Additionally, the experimental waveforms of the voltages and currents are measured by an oscilloscope (YOKOGAWA DLM2054).

TABLE II
CASE STUDY FOR PARAMETER ESTIMATION

Case No.	D [cm]	L_P [μH]	L_S [μH]	M [μH]	C_P [nF]	C_S [nF]
Case-I	10	335.5	222.7	95	9.9	17.32
Case-II	10	335.5	222.7	95	11.53	16.5
Case-III	10	335.5	222.7	95	9.9	13.21
Case-IV	15	327.5	216.5	58	9.9	17.32
Case-V	15	327.5	216.5	58	11.53	16.5

TABLE III
PARAMETERS OF THE JAYA ALGORITHM

Symbol	Value	Symbol	Value	Symbol	Value
L_{PL}	300 μH	L_{PH}	350 μH	L_{SL}	200 μH
L_{SH}	250 μH	M_L	50 μH	M_H	120 μH
C_{PL}	5 nF	C_{PH}	15 nF	C_{SL}	10 nF
C_{SH}	20 nF	R_{PL}	0.5 Ω	R_{PH}	0.9 Ω
R_{SL}	0.3 Ω	R_{SH}	0.7 Ω	P_{size}	50
Gen_{max}	5000				

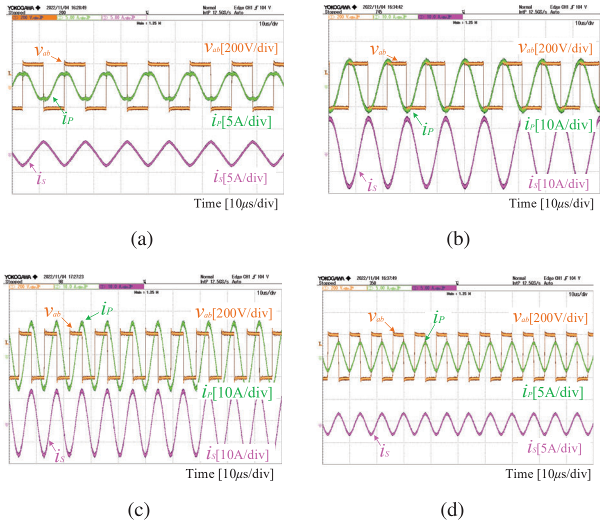

(a) (b)

(c) (d)

Fig. 9. Experimental results of case-I under various frequencies: (a) 65.0 kHz, (b) 70.4 kHz, (c) 107.7 kHz, (d) 125.0 kHz.

To validate the accuracy of the proposed method, 5 different cases of parameter deviations are investigated. The detailed parameters of the studied 5 cases are shown in Table. II. These parameters are previously measured by an impedance analyser (Agilent 4294A). The estimated results will then compared with the measured values to verify the estimation accuracy.

Firstly, in order to obtain the required data for the estimation, the operating frequency f is dynamically adjusted

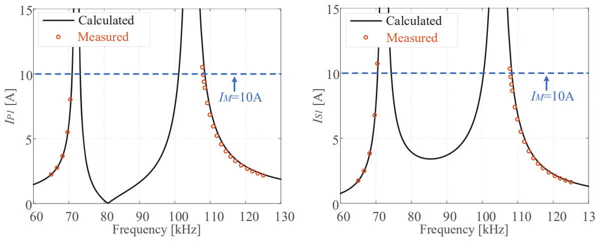

(a) (b)

Fig. 10. Measured coil currents of case-I: (a) I_{P1}, (b)I_{S1}.

TABLE IV
AVERAGE RELATIVE ERRORS (ARES) OF THE INVESTIGATED CASES IN THE EXPERIMENTS

Case No.	L_P	L_S	C_P	C_S	M
Case-I	1.56%	1.37%	0.9%	1.85 %	0.41%
Case-II	1.27%	0.21%	0.99%	0.52%	0.25%
Case-III	2.19%	**2.67%**	1.52%	2.02 %	2.2 %
Case-IV	0.73%	2.08%	0.56%	1.82 %	0.16%
Case-V	0.98 %	1.9%	0.62%	1.68%	0.27%

according to the update formulas (6) and (7). Fig. 9 presents the measured operating waveforms of case-I under different frequency points. The measured data from the oscilloscope is further exported to MATLAB for data analysis. Two digital LPFs are utilized to extract the fundamental components of i_P and i_S, respectively. Subsequently , the RMS values of i_{P1} and i_{S1} are calculated. Fig. 10 further shows the extracted RMS values of case-I. By implementing the proposed dynamic frequency sweeping frequency method, as shown in Fig. 10, I_{P1} and I_{S1} are accurately measured under multiple frequency points. Finally, according to the measured data, the JAYA algorithm is carried out in MATLAB to derive the optimal solutions described in (5). The detailed parameters of the JAYA algorithm are shown in Table. III.

In the experiments, the JAYA algorithm is implemented for 10 times for each case, and the average relative errors (AREs) for the investigated 5 cases are illustrated in Table IV. As shown in Table IV, the unknown parameters of the resonant circuits are recognized accurately, with the maximum AREs at 2.67%.

V. CONCLUSIONS

This paper presents a new parameter estimation strategy for the WPT systems. To prevent significant load power fluctuations, the active rectifier is short-circuited during the parameter estimation process. Since the proposed method is free of the load conditions, it can be implemented at the pre-start-up stage in the practical applications. Notably, as the proposed method requires freqeuncy sweeping and numerical calculations, it may take several seconds to complete the entire process for parameter estimation. As a consequence, this method is not suitable for real-time dynamic prediction, but more suitable for static battery charging. With a short-circuited rectifier, a dynamic frequency sweeping method is further proposed to efficiently and safely measure the primary and secondary coil currents. Based on the extracted data, a mathematical model is established, and the JAYA algorithm is adopted to find the optimal solutions. Experimental results show that the proposed method is able to accurately estimate all of the unknown parameters of the resonant circuits. The proposed method is beneficial for optimal power flow control and active impedance tuning for the WPT systems under parameter deviations.

REFERENCES

[1] S. Hui, "Planar wireless charging technology for portable electronic products and qi," *Proceedings of the IEEE*, vol. 101, no. 6, pp. 1290–1301, 2013.
[2] R. Guida, E. Demirors, N. Dave, and T. Melodia, "Underwater ultrasonic wireless power transfer: A battery-less platform for the internet of underwater things," *IEEE Transactions on Mobile Computing*, vol. 21, no. 5, pp. 1861–1873, 2020.
[3] Q. Wang, W. Che, M. Mongiardo, and G. Monti, "Wireless power transfer system with high misalignment tolerance for bio-medical implants," *IEEE Transactions on Circuits and Systems II: Express Briefs*, vol. 67, no. 12, pp. 3023–3027, 2020.
[4] G. Yu, J. Dong, T. B. Soeiro, G. Zhu, Y. Yao, and P. Bauer, "Three-mode variable-frequency zvs modulation for four-switch buck+ boost converters with ultra-high efficiency," *IEEE Transactions on Power Electronics*, vol. 38, no. 4, pp. 4805–4819, 2022.
[5] W. Zhang and C. C. Mi, "Compensation topologies of high-power wireless power transfer systems," *IEEE Transactions on Vehicular Technology*, vol. 65, no. 6, pp. 4768–4778, 2015.
[6] D.-H. Kim and D. Ahn, "Self-tuning lcc inverter using pwm-controlled switched capacitor for inductive wireless power transfer," *IEEE Transactions on Industrial Electronics*, vol. 66, no. 5, pp. 3983–3992, 2018.
[7] J. Yin, D. Lin, C. K. Lee, T. Parisini, and S. Hui, "Front-end monitoring of multiple loads in wireless power transfer systems without wireless communication systems," *IEEE Transactions on Power Electronics*, vol. 31, no. 3, pp. 2510–2517, 2015.
[8] J. Yin, D. Lin, T. Parisini, and S. Hui, "Front-end monitoring of the mutual inductance and load resistance in a series–series compensated wireless power transfer system," *IEEE Transactions on Power Electronics*, vol. 31, no. 10, pp. 7339–7352, 2015.
[9] Y. Yang, S.-C. Tan, and S. Y. R. Hui, "Front-end parameter monitoring method based on two-layer adaptive differential evolution for ss-compensated wireless power transfer systems," *IEEE Transactions on Industrial Informatics*, vol. 15, no. 11, pp. 6101–6113, 2019.
[10] D. Lin, J. Yin, and S. R. Hui, "Parameter identification of wireless power transfer systems using input voltage and current," in *2014 IEEE energy conversion congress and exposition (ECCE)*. IEEE, 2014, pp. 832–836.
[11] W. Xiao, R. Shen, B. Zhang, D. Qiu, Y. Chen, and F. Xie, "Multiple parameters estimation based on transmitter side information in wireless power transfer system," *IEEE Access*, vol. 7, pp. 164 835–164 843, 2019.
[12] G. Zhu, J. Dong, W. Shi, T. B. Soeiro, J. Xu, and P. Bauer, "A mode-switching based phase shift control for optimized efficiency and wide zvs operations in wireless power transfer systems," *IEEE Transactions on Power Electronics*, 2022.
[13] M. Mohammad, O. C. Onar, G.-J. Su, J. Pries, V. P. Galigekere, S. Anwar, E. Asa, J. Wilkins, R. Wiles, C. P. White *et al.*, "Bidirectional lcc–lcc-compensated 20-kw wireless power transfer system for medium-duty vehicle charging," *IEEE Transactions on Transportation Electrification*, vol. 7, no. 3, pp. 1205–1218, 2021.
[14] R. Mai, Y. Liu, Y. Li, P. Yue, G. Cao, and Z. He, "An active-rectifier-based maximum efficiency tracking method using an additional measurement coil for wireless power transfer," *IEEE Transactions on Power Electronics*, vol. 33, no. 1, pp. 716–728, 2017.
[15] G. Zhu, J. Dong, F. Grazian, and P. Bauer, "A parameter recognition based impedance tuning method for ss-compensated wireless power transfer systems," *IEEE Transactions on Power Electronics*, 2023.
[16] R. Rao, "Jaya: A simple and new optimization algorithm for solving constrained and unconstrained optimization problems," *International Journal of Industrial Engineering Computations*, vol. 7, no. 1, pp. 19–34, 2016.